RSC Advances

ROYAL SOCIETY OF CHEMISTRY

www.rsc.org/advances

Six lanthanide complexes based on 5-azotetrazolyl salicylic acid were synthesized and their crystal structures, magnetic and photochromic properties were reported.

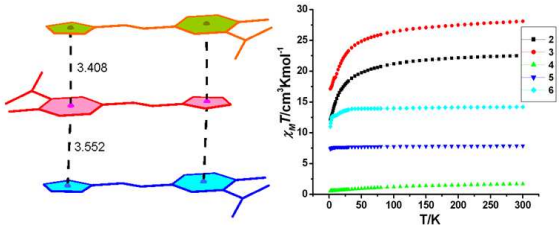

Journal Name

RSCPublishing

ARTICLE

Syntheses, Supramolecular Structures, Magnetic and Photochromic Properties of Six Lanthanide Complexes Based on 5-Azotetrazolyl Salicylic Acid Ligand

Cite this: DOI: 10.1039/x0xx00000x

Received ooth January 2012,
Accepted ooth January 2012

DOI: 10.1039/x0xx00000x

www.rsc.org/

Wen-Bin Chen, Zhi-Xin Li, Zhi-Jian Ouyang, Wen-Ning Lin, Liu Yang and Wen Dong*

Six lanthanide complexes based on 5-azotetrazolyl salicylic acid (H_3ASA) ligand of $\{[Er(H_2ASA)(HASA)(H_2O)_6]\cdot 6H_2O\}$ (**1**), $\{[Ln(H_2ASA)(HASA)(H_2O)_4]_2\cdot 6H_2O\}$ [Ln = Er (**2**), Ho (**3**)], $[Ln(H_2ASA)(HASA)(H_2O)_4]$ [Ln = Nd (**4**), Gd (**5**)] and $\{[Dy(ASA)(H_2O)_5]\cdot 5H_2O\}$ (**6**) have been synthesized and characterized by single crystal X-ray diffraction analysis. In **1**–**6**, the carboxyl group act as different coordinating or bridging modes resulting in a mononuclear structure for **1**, two dinuclear structures for **2** and **3** and three one-dimensional structures for **4**-**6**, and the unusual π^-–π stacking between tetrazolate anions and phenyl rings and various hydrogen bonding interactions are observed. The energies for π^-–π stacking interactions were calculated and demonstrated at MP_2 level using Gaussion 09 suite. The magnetic properties of **2**–**6** and photochromism for aqueous solutions of **1**–**6** were investigated.

Introduction

Currently, the assembly of various novel transition or lanthanide metal complexes with optical, electrical and magnetic properties give rise to considerable interest among researchers due to their potential applications as functional materials.[1] An efficient approach for generation of such type of functional complexes is to assemble appropriate organic ligands into different metal systems by coordination bond and the assist of noncovalent intermolecular π–π stacking and hydrogen bonding interactions.[2-5] Because ligands can control the structures and properties of the complexes by different coordinating and bridging modes, the judicious choice and design of appropriate ligands containing varied functional groups is particularly important for synthetic strategy. Carboxylates have been proven to be excellent ligands in the design and construction of magnetic and optical functional lanthanide complexes, because they can coordinate to Ln(III) ions through monodentate, bidentate, and tridentate types of coordination modes and efficiently transmit energy and magnetic coupling by carboxyl bridge.[6] Among the carboxylates, salicylic acid and its derivatives are particularly desirable ligands because both carboxyl and phenolic hydroxyl groups in salicylate ligands can act as bridges or take part in the formation of intra- and/or intermolecular hydrogen bonds to assist the formation of multidimensional assemblies.[1h,7] Despite the extensive investigations carried out on various carboxylate analogues, studies on metal complexes of 5-azotetrazolyl salicylic acid (H_3ASA) are rare.[8] The H_3ASA is one of especially desirable organic functional ligand, because it possesses carboxyl, hydroxyl, azo, and tetrazole functional moieties, and can not only be partly (H_2ASA^- and $HASA^{2-}$) or fully (ASA^{3-}) deprotonated but also exhibit trans-cis isomers originating from photoisomerization reactions of azo linker (Scheme 1).[8a] Azo functional linker is known to all to be an efficient electronic bridge, which prompts the creation of

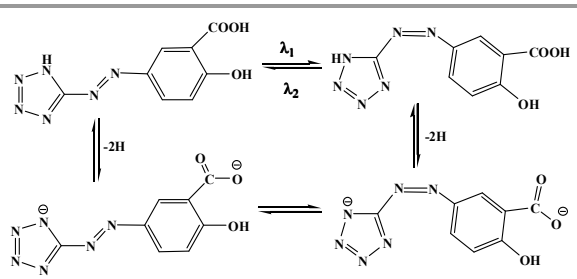

Scheme 1. The doubly deprotonated and photoisomerization reactions of H_3ASA.

extended-conjugated systems, and azo based compounds can undergo reversible trans-cis isomerization and show photochromic property upon light irradiation.[9] Very recently, the pronounced bathochromic absorption and photochromism for azo based compounds including 1,1'–azobis-1,2,3–triazole, 1,1'–azobis-tetrazole and 5,5'–azotetrazolate based complexes were reported.[10] Here, six Ln(III) complexes based on H_3ASA ligand of **1-6** were synthesized and their crystal structures, magnetic and photochromic properties were reported.

Experimental Section

Materials and Physical Measurements

All the commercial reagents and solvents were used without further purification unless otherwise stated. IR spectra were recorded as pressed KBr pellets on a Bruker Tensor 27 spectrophotometer. Elemental analyses for C, H and N were performed on a Perkin-Elmer 240 CHN elemental analyzer. The magnetic measurements of the sample of **2-6** were carried out using a SQUID magnetometer in the temperature range of 2–300 K at a constant magnetic field (1000 Oe). UV-vis absorption spectra of **1-6** in aqueous solution were recorded with a U-1800 Ultraviolet-Visible Spectrophotometer.

X-ray crystallography and data collection

The crystals were filtered from the solution and immediately coated with hydrocarbon oil on the microscope slide. Suitable crystals were mounted on glass fibers with silicone grease and placed in a Bruker Smart APEX(II) area detector using graphite monochromated Mo-Kα radiation (λ = 0.71073 Å) at 296(2) K. The structures were solved by direct methods and successive Fourier difference syntheses (SHELXS-97) and refined by full–matrix least-squares procedure on F^2 with anisotropic thermal parameters for all non-hydrogen atoms (SHELXL-97). Organic hydrogens were generated geometrically (C-H 0.96 Å); hydrogen atoms in the azotetrazolyl and in the water molecules were located from difference maps and refined with isotropic temperature factors. In **5**, two N atoms in azo bond were found to be disordered over two positions with an occupancy factor of 0.500/0.500 (N7 and N8), 0.500/0.500 (N13 and N14). Although routine checks strongly suggested that the space group for **4** and **5** should be the centrosymmmetric C2/c space group instead of the reported Cc. This would place the metal atom on a twofold axis in the C2/c space group, but would result in significant H_3ASA ligand disorder. Crystallographic data has been deposited in the Cambridge Crystallographic Database Centre: CCDC 975945 for **1**, 975946 for **2**, 993757 for **3**, 975949 for **4**, 993758 for **5**, 993759 for **6**. The summary of crystallographic data and structural refinements for **1**–**6** should read Table 1.

Computational details

All the quantum-chemical calculations were done with the Gaussian 09 suite.[11] The calculations of π^-–π interactions were performed using MP2 at 6-31G level based on the crystal structures obtained in this work. The interaction energies were counterpoise corrected with the procedure of Boys and Bernardi, in order to account for the basis set superposition error (BSSE).[12]

Synthesis of H_3ASA

5-azotetrazolyl salicylic acid was synthesized according to the reported method in reference.[13]

Synthesis of {[Er(H_2ASA)(HASA)(H_2O)$_6$]·6H_2O} (1)

10 mL aqueous solution of Er_2O_3 (0.0382 g, 0.1 mmol) and HCl (6 mol·L^{-1}, 2d) was added to a solution of 5-azotetrazolyl salicylic acid (0.0504 g, 0.2 mmol) in 10 mL of water and 10 mL of ethanol and stirred for 2 h. The pH of mixture solution is about 4. The resulting mixture was filtered. The filtrate was allowed to evaporate slowly under ambient conditions for several days. The obtained yellow crystals were isolated by suction filtration and washed with ethanol. Yield: 56.61% (based on Er^{3+}). Anal. Calcd. for **1** of $C_{16}H_{33}N_{12}O_{18}Er$ (%): C, 22.62; H, 3.89; N, 19.79. Found(%): C, 22.53; H, 3.93; N, 19.75. FT-IR (KBr, cm^{-1}): 3193s, 1678m, 1631m, 1580s, 1539s, 1486s, 1444s, 1385s, 1258s, 1179s, 901m, 835m, 808m, 681s, 562m.

Syntheses of {[Ln(H_2ASA)(HASA)(H_2O)$_4$]$_2$·6H_2O} [Ln = Er (2), Ho (3)]

10 mL aqueous solution of MCl_3·6H_2O (0.1 mmol) was added to a solution of 5-azotetrazolyl salicylic acid (0.0504 g, 0.2 mmol) in 10mL of water and 10mL of ethanol and stirred for 5 min. Then a drop of dilute NH_3·H_2O (2 mol·dm^{-3}) was added to adjust the pH to about 5 and stirred for 2 h. The resulting mixture was filtered and block crystals were obtained by slow evaporation of the filtrate after several days and washed with ethanol with yields of 42.31% for **2** (based on Er^{3+}), 39.82% for **3** (based on Ho^{3+}). Anal. Calcd. for **2** of $C_{32}H_{46}N_{24}O_{26}Er_2$ (%): C, 25.31; H, 3.03; N, 22.14. Found(%): C, 25.29; H, 3.09; N, 22.10. FT-IR (KBr, cm^{-1}): 3209s, 1676m, 1629s, 1580s, 1487s, 1443s, 1385s, 1259m, 1178s, 835m, 681s, 561m for **2**. Anal. Calcd. for **3** of $C_{32}H_{46}N_{24}O_{26}Ho_2$(%): C, 25.38; H, 3.04; N, 22.21. Found(%): C, 25.39; H, 3.01; N, 22.26. FT-IR (KBr, cm^{-1}): 3190s, 1605s, 1547s, 1487m, 1419s, 1394s, 1333s, 1271s, 1188s, 1151s, 1082m, 838m, 758s, 671m, 613m, 577m.

Syntheses of [Ln(H_2ASA)(HASA)(H_2O)$_4$] [Ln = Nd (4), Gd (5)]

10 mL aqueous solution of MCl_3·6H_2O (0.1 mmol) was added to a solution of 5-azotetrazolyl salicylic acid (0.0504 g, 0.2 mmol) in 10mL of water and 10mL of ethanol and stirred for 5 min. Four drop of dilute NH_3·H_2O (2 mol·dm^{-3}) was added to the mixture solution. And then dilute HCl (2 mol·dm^{-3}) was added to adjust the pH to about 6 and stirred for 2 h. The resulting mixture was filtered. Yellow block crystals of **4** and yellow block crystals of **5** formed in the filtrate by slow evaporation of the solvents within several days and were isolated by filtration. Yields: 41.2% for **4** (based on Nd^{3+}) and 32.5% for **5** (based on Gd^{3+}). Anal.Calcd. for **4** of $C_{16}H_{17}N_{12}O_{10}Nd$ (%): C, 28.17; H, 2.49; N, 24.65. Found(%): C,

28.16; H, 2.48; N, 24.63. FT-IR (KBr, cm^{-1}):3319s, 1624m, 1562s, 1466s, 1387s, 1247s, 1149m, 1031m, 850m, 805m, 754s, 702m, 664s, 570m, 528m for **4**. Anal. Calcd. for **5** of $C_{16}H_{17}N_{12}O_{10}Gd$ (%): C, 27.64; H, 2.45; N, 24.18. Found(%): C, 27.69; H, 2.42; N, 24.19. FT-IR (KBr, cm^{-1}): 3213s, 1672m, 1625m, 1580s, 1537s, 1483s, 1442s, 1385s, 1258s, 1177s, 901m, 836m, 807m, 682m, 562m, 523w.

Synthesis of {[Dy(ASA)$(H_2O)_5$]·$5H_2O$} (6)

10 mL aqueous solution of $Dy(OAc)_3·10H_2O$ (0.1 mmol) was added to a solution of 5-azotetrazolyl salicylic acid (0.0252 g, 0.2 mmol) in 10mL of water and 10mL of ethanol and stirred for 5 min. Four drop of dilute $NH_3·H_2O$ (2 mol·dm^{-3}) was added to the mixture solution. And then dilute HCOOH (2 mol·dm^{-3}) was added to adjust the pH to about 7 and stirred for 2 h and filtered. The filtrate was allowed to evaporate slowly under ambient conditions, and yellow crystals suitable for X-ray analysis were obtained by slow evaporation of the solvents within several days. Yields: 29.5% for **6** (based on Dy^{3+}), Anal. Calcd. for **6** of $C_8H_{23}DyN_6O_{13}$ (%): C, 16.73; H, 4.01; N, 14.64. Found(%): C, 16.84; H, 3.96; N, 14.73. FT-IR (KBr, cm^{-1}): 3203s, 1606s, 1549m, 1524w, 1485s, 1421s, 1334s, 1266s, 1189s, 1152m, 1084w, 841m, 760m, 675m, 615w, 577m, 532w for **6**.

Results and discussion

Crystal structure of 1

Table 1 gives crystallographic data for complexes of **1**–**6**. Complex **1** crystallizes in the triclinic space group Pī. Each Er^{3+} coordinates to four carboxyl oxygen atoms from two anionic ligands of $HASA^{2-}$ and H_2ASA^- and six oxygen atoms from water molecules to give an eight-coordinated square antiprism (Fig. 1a). The H_2ASA^- and $HASA^{2-}$ anions show a monodentate ligand and **1** displays a mononuclear structure. The bond lengths of C2-O3 (phenol) = 1.342(3) Å and C10-O6 (phenol) = 1.334(3) Å indicate an enol isomer for H_2ASA^- and $HASA^{2-}$ anions. A slipped face-to-face alignment between tetrazolate anions and phenyl aromatic rings with the separated interplanar center to center distances of 3.496(2) and 3.711(2) Å, behaves as a unusual π^-–π stacking interactions in **1** (Fig. 1b). Another edge-to-face π–π stacking interactions are also observed with

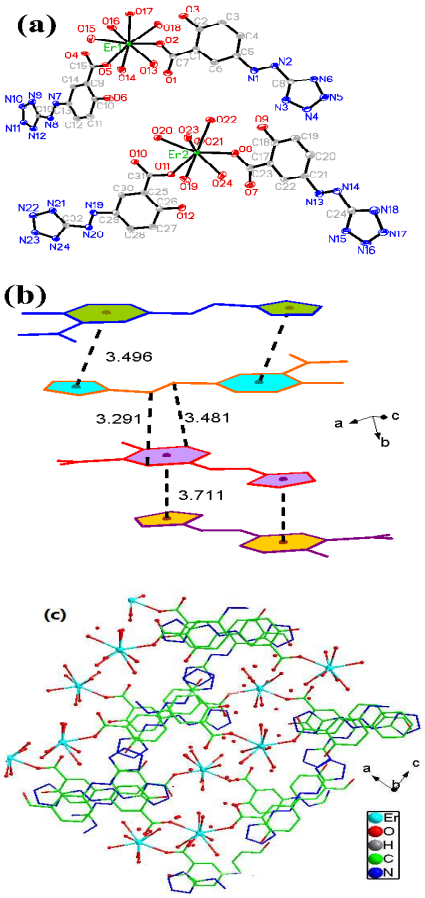

Fig. 1 (a) ORTEP view (30% thermal ellipsoids) of **1**, all H atoms and lattice water molecules have been omitted for clarity, (b) the π^-–π stacking interaction in **1**, (c) the 3D supramolecular structure of **1**.

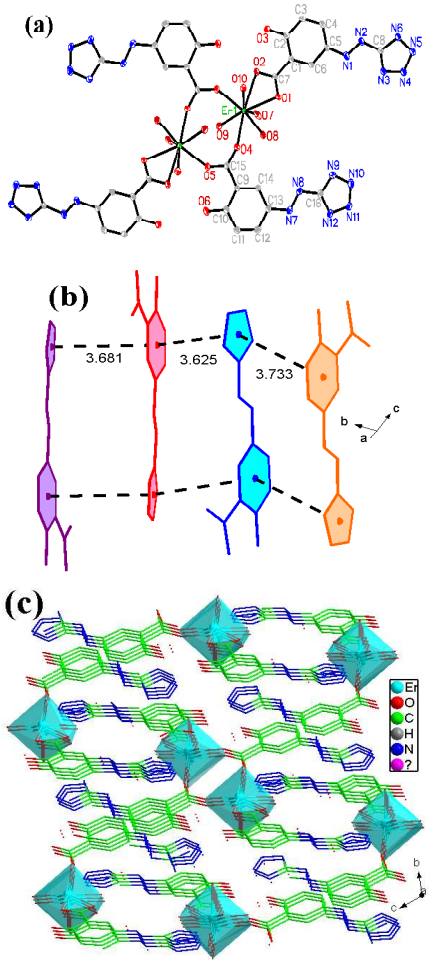

Fig. 2 (a) ORTEP view (30% thermal ellipsoids) of **2**, all H atoms and lattice water molecules have been omitted for clarity, (b) the π^-–π stacking interaction in **2**, (c) the 3D supramolecular structure of **2**.

the shortest atom-to-atom distances of 3.291(4) and 3.481(4) Å.There are five kinds of hydrogen-bonds of O–H···O (carboxyl), O–H···O (hydroxyl), O–H···N, O–H···O (lattice water molecules) and O–H···O (coordination water molecules) among the H_2ASA^-, $HASA^{2-}$ anionic ligands, lattice water molecules and solvent water molecules (Fig. S1, ESI†). The shortest distances of O–H···O (carboxyl), O–H···O (hydroxyl) are 2.734(3) and 2.873(3) Å, respectively. The π^-–π stacking and hydrogen bonding interactions are responsible for the stabilization of 3D supramolecular structure (Fig. 1c).

Crystal structures of 2 and 3

Single-crystal X-ray analysis reveal that complexes **2** and **3** are isomorphous and the crystal structure of **2** is described as the example. Complex **2** crystallizes in the triclinic space group P$\bar{1}$ with each unit cell consisting of two Er^{3+} ions, two H_2ASA^- anion, two $HASA^{2-}$ anion, four coordination water molecules and three lattice water molecules (Fig. 2a). Each Er^{3+} ion coordinates to eight oxygen atoms, including four carboxylic oxygen atoms from two μ_2 bridging $HASA^{2-}$ anions and a chelating bidentate H_2ASA^- anion and four oxygen atoms of water molecules. The coordination geometry around the metal center can be described as a distorted square antiprism. The dimeric compound lies about an inversion center. Two μ_2 bridging carboxylic groups links two Er^{3+} ions to give a dinuclear structure with the separation of $Er^{3+}\cdots Er^{3+}$ distance of 4.929(7) Å (Fig. 2a). The dihedral angles between the tetrazole and phenyl ring of H_2ASA^- and $HASA^{2-}$ anions are 7.96(9)° and 1.78(9)°, respectively, which indicate an approximately coplanar structure. A slipped face-to-face π^-–π stacking interaction is observed between tetrazolate anions and phenyl aromatic rings with the separated interplanar center to center distances ranging from 3.625(5) to 3.733(6)Å (Fig. 2b). There are six kinds of hydrogen-bonds of O–H···O (carboxyl), O–H···O (hydroxyl), O–H (hydroxyl)···O (carboxyl), O–H···N, O–H···O (lattice water molecules) and O–H···O (coordination water molecules) among the H_2ASA^-, $HASA^{2-}$ anionic ligands, lattice water molecules and solvent water molecules (Fig. S2, ESI†). The distances of O–H···O (carboxyl), O–H···O (hydroxyl) and O–H(hydroxyl)···O (carboxyl) are 2.885 (5), 2.860(3) and 2.998(3) Å, respectively. The π^-–π stacking and hydrogen bonding are responsible for the stabilization of 3D supramolecular structures (Fig. 2c).

Crystal structure of 4 and 5

X-ray diffraction analysis reveals that **4** and **5** are isomorphic. So, **4** is employed as a representative complex to be described in detail. It crystallizes in the monoclinic system and space group Cc. As shown in Fig. 3a, an asymmetric unit of **4** consists of a Nd^{3+} ion, a H_2ASA^- anion, a $HASA^{2-}$ anion and four coordination water molecules. Each Nd^{3+} ion coordinates to eight oxygen atoms from four carboxylic oxygen atoms from two H_2ASA^- anion and two $HASA^{2-}$ anion ligands and four oxygen atoms from four water molecules to give a distorted square antiprism. The dihedral angle between the tetrazolate rings and phenyl aromatic rings of H_2ASA^- and $HASA^{2-}$ are 18.66(43)° and 13.49(44)°, respectively. Both H_2ASA^- and two $HASA^{2-}$ anions act as μ_2 bridging ligands with each anion links two different Nd^{3+} ions to give one dimensional linear chain structure with the separation of $Nd^{3+}\cdots Nd^{3+}$ distance of 5.067(1) Å. A face-to-face alignments between the tetrazolate anions and phenyl aromatic rings with the separated interplanar center-to-center distances of 3.755(1) Å is observed, which displays a π^-–π stacking interactions (Fig. 3b). Another edge-to-face π–π stacking interactions are also observed with the shortest atom-to-atom distances of 3.211(17) and 3.454(17) Å. Four coordination water molecules are linked with nitrogen atoms in tetrazolyl by the O–H···N hydrogen-bonds with the O···N distances of 2.711(10) to 2.968(12) Å (Fig. S3, ESI†). The π^-–π stacking and O–H···N hydrogen bonding interactions link the 1D structures into a 3D supramolecular structure (Fig. 3d).

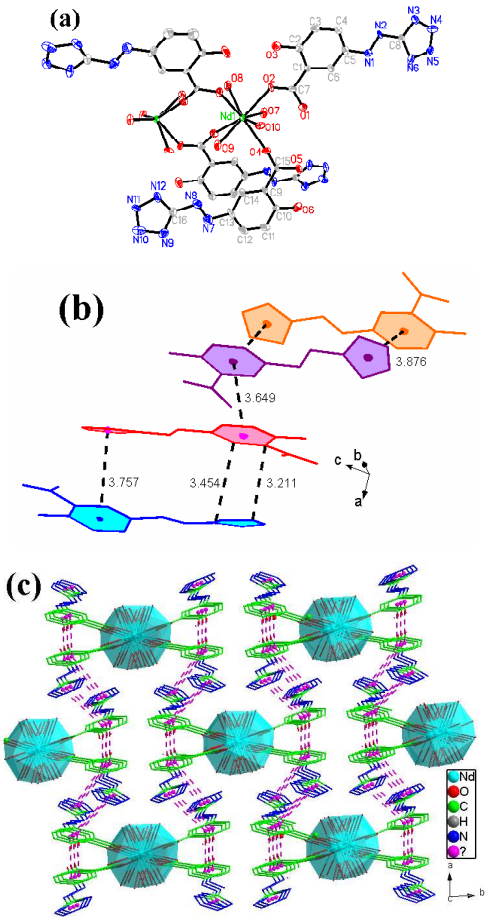

Fig. 3 (a) ORTEP view (30% thermal ellipsoids) of **4**, all H atoms have been omitted for clarity, (b) the π^-–π stacking interaction in **4**, (c) the 3D supramolecular structure showing the π^-–π stacking interaction.

Crystal structure of 6

Complex **6** crystallizes in the monoclinic space group P21/n. Fig. 4a gives its atomic labeling diagram. Each Dy^{3+} coordinates to a phenolate, two carboxylate oxygen atoms and four water molecules to give a distorted eight-coordinated square antiprism. In this complex, the ASA^{3-} anion behaves as a

μ_2 bridging ligand coordinating to two different Dy^{3+} ions with the separation of $Dy^{3+}\cdots Dy^{3+}$ being 5.817(5) Å, resulting in a 1D zigzag chain structure. The ASA^{3-} anions show trans-enol-E isomers. The dihedral angle between the tetrazolate anionic rings and phenyl aromatic rings of ASA^{3-} is 5.07(15)°. A face-to-face π^{-}–π stacking interaction between the tetrazolate anionic and phenyl rings with the separated interplanar center-to-center distances of 3.408(5) to 3.552(5) Å in ASA^{3-} anions is also observed (Fig. 4b). Four kinds of hydrogen-bonds of O–H···O (hydroxyl), O–H···N, O–H···O (lattice water molecules) and O–H···O (coordination water molecules) among the ASA^{3-} anionic ligands, lattice water molecules and solvent water molecules are also observed in **6** with shortest distances of 2.685(5), 2.687(5), 2.729(18) and 2.750(7) Å, respectively (Fig. S6, ESI†). A cage-shaped dodecameric water cluster of $(H_2O)_{12}$ with the O···O distance range of 2.648(12) to 2.990(64) Å is found and shown in Fig. 4c. The O–O–O angles in this $(H_2O)_{12}$ cluster range from 80.6(5)–119.8(3)°. The dodecameric water cluster described here is different from previously identified cyclic ring structures and other cage-like structures, which represents a novel conformation of $(H_2O)_{12}$ cluster not yet predicted.[14] In this complex, the π^{-}–π stacking together with the O···N and O···O hydrogen bonding interactions link the 1D complex chain into a 3D supramolecular network structure (Fig. 4d).

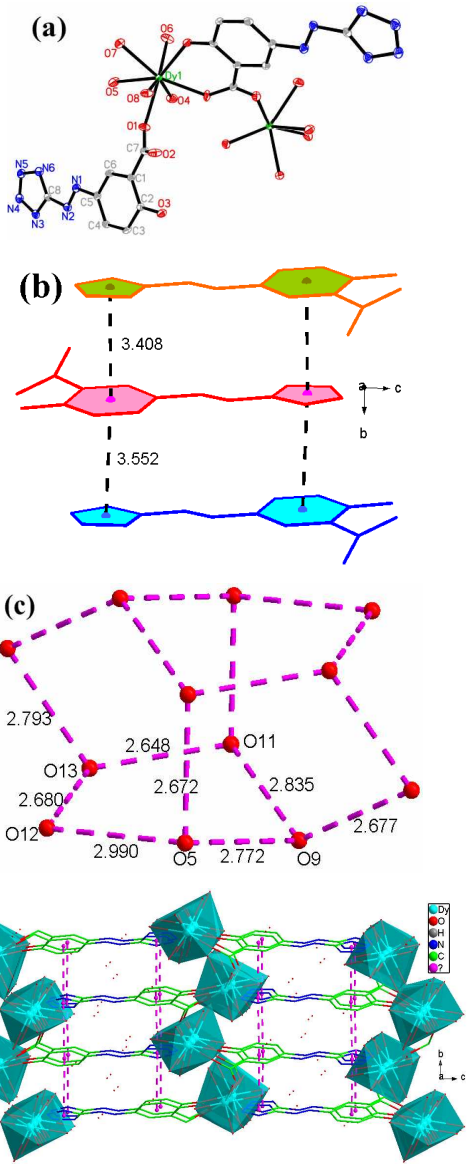

Fig. 4 (a) ORTEP view (30% thermal ellipsoids) of **7**, all H atoms and lattice water molecules have been omitted for clarity, (b) the π^{-}–π stacking interaction in **7**, (c) the structure of cage-shaped water cluster of $(H_2O)_{12}$ in **7**, (d) the 3D supramolecular structure showing the π^{-}–π stacking interaction..

Comparison of the structures

Different methods of synthesis were used to prepare complexes **1**–**6**, so complexes with different structures were obtained, especially for **1**, which has mononuclear structure, for **2** and **3**, which have dinuclear structures, for **4** and **5**, which have one-dimensional structures while **6** also has an one-dimensional structure in which hydroxyl group coordinates to Dy(III) ion. When preparing **1**, H_3ASA and rare earth oxides with hydrochloric acid replacing rare earth salts were used and the pH of reaction solution was 4. When preparing **2** and **3**, H_3ASA and rare earth salts were used and the pH of reaction solution was adjusted to about 5. H_3ASA and rare earth salts were also used in preparing **4** and **5**, while the pH of reaction solution was adjusted to about 6. The H_3ASA ligand were not completely deprotonated in **1**–**5** because of the acidic reaction solution. However, when the pH of reaction solution for preparing complex **6** was adjusted to 7, H_3ASA was deprotonated completely, which increased the coordination opportunity of the H_3ASA ligand. It indicates that the solution acidity might play important role in designing and synthesising different structure complexes.[15]

The energies for π^{-}–π stacking interactions in 1-6

As shown in Table 2, the calculated π^{-}–π interaction energies between tetrazolate anions and phenyl aromatic rings in **1-6** range from -16.2457 to -43.8113 kJ·mol^{-1} which are stronger than the general π–π interactions.[16] The results clearly demonstrate that the π–π interactions increase the likelihood of formation of π–π stacked crystal structures.

Table 2 The structural parameters and interaction energies of **1-6**

Complex	Distance(center to centre)(Å)[a]	Energy (kJ·mol^{-1})
1	3.496	-16.2457
2	3.626	-43.8113
3	3.633	-30.5457
4	3.755	-41.4081
5	3.772	-40.4960
6	3.550	-32.8837

[a]centre of tetrazolate anions ring to centre of phenyl aromatic ring

Magnetic properties

{[Er(H$_2$ASA)(HASA)(H$_2$O)$_4$]$_2$·6H$_2$O} (2). The temperature dependence of magnetic susceptibilities of **2-6** have been measured on microcrystalline samples over the temperature range 2−300 K under an applied direct current (dc) magnetic field of 1000 Oe. The $\chi_M T$ and χ_M versus T plots for Complex **2** are shown in Fig. 5. The $\chi_M T$ value for **2** at 300K is 22.49 cm^3 K mol^{-1}, which is close to the value expected for two noninteracting Er^{3+} ions ($^4I_{15/2}$, S = 3/2, L = 6, g = 6/5, $\chi_M T$ = 11.48 cm^3 K mol^{-1}). Upon cooling, the $\chi_M T$ value gradually decreases and reaches a minimum of 12.09 cm^3 K mol^{-1} at 2 K. The lowering of $\chi_M T$ values with decreasing temperature may arise from the depopulation of Stark sublevels and/or antiferromagnetic interactions between the Er^{3+} ions in **2**. The feasible fit of the experimental data for the plot of χ_M vs. T in the range 50–300 K, following the Curie–Weiss law [χ_M = C/(T -θ) + χ_0], yielded the Curie constant C = 22.726 cm^3 K mol^{-1}, the Weiss constant θ = -8.019 K, and the background susceptibility χ_0 = 0.00138 cm^3 mol^{-1}. To estimate the magnetic exchange coupling constant, the dinuclear structure is modelled with the spin Hamiltonian:

$$\hat{H} = -2J\hat{S}_1\hat{S}_2 = -J(\hat{S}_T^2 - \sum_{i=1}^{2}\hat{S}^2)$$

$$\chi = \frac{Ng^2\beta^2}{3kT} \times \frac{\begin{array}{l}7440e^{240J/kT} + 6090e^{210J/kT} + 4914e^{182J/kT} + 3900e^{156J/kT} \\ + 3036e^{132J/kT} + 2310e^{110J/kT} + 1710e^{90J/kT} + 1224e^{72J/kT} + 840e^{56J/kT} \\ + 546e^{42J/kT} + 330e^{30J/kT} + 180e^{20J/kT} + 84e^{12J/kT} + 30e^{6J/kT} + 6e^{2J/kT}\end{array}}{\begin{array}{l}31e^{240J/kT} + 29e^{210J/kT} + 27e^{182J/kT} + 25e^{156J/kT} + 23e^{132J/kT} + 21e^{110J/kT} \\ + 19e^{90J/kT} + 17e^{72J/kT} + 15e^{56J/kT} + 13e^{42J/kT} + 11e^{30J/kT} + 9e^{20J/kT} \\ + 7e^{12J/kT} + 5e^{6J/kT} + 3e^{2J/kT} + 1\end{array}}$$

$$\chi_{Er} = \frac{\chi}{1-(2zj'/Ng^2\beta^2)\chi}$$

In these expressions, J is magnetic exchange coupling constant, N, g, β, and k have their usual meanings, zJ' is the total exchange parameter. The best fitting of the susceptibility data in the temperature range 50–300 K gives J = -0.107 cm^{-1}, zJ' = -3.930×10^{-4} cm^{-1}, g = 1.187, R = $\Sigma[(\chi T)_{obsd} - (\chi T)_{calcd}]^2/\Sigma[(\chi T)_{obsd}]^2$ = 2.039×10^{-6}. The negative value of zJ' and θ indicate the presence of weak antiferromagnetic interactions between Er^{3+} ions.

{[Ho(H$_2$ASA)(HASA)(H$_2$O)$_4$]$_2$·6H$_2$O} (3). Complex **3** present a similar magnetic behavior to complex **2** (Fig. 6). The $\chi_M T$ value for **3** at 300K is 28.08 cm^3 K mol^{-1}, which is close to the value expected for two noninteracting Ho^{3+} ions ($^5I_8$, S = 2, L = 6, g = 5/4, $\chi_M T$ = 14.08 cm^3 K mol^{-1}). Upon cooling, the $\chi_M T$ value gradually decreases and reaches a minimum of 17.12 cm^3 K mol^{-1} at 2 K. The decrease of the $\chi_M T$ values when lowering the temperature may arise from the depopulation of Stark sublevels and/or antiferromagnetic interactions between the Ho^{3+} ions in **3**. The feasible fit of the experimental data for the plot of χ_M vs. T in the range 50–300 K, following the Curie–Weiss law [χ_M = C/(T -θ) + χ_0], yielded the Curie constant C = 27.632 cm^3 K mol^{-1}, the Weiss constant θ = -6.073 K, and the background susceptibility χ_0 = 0.0033 cm^3 mol^{-1}. To estimate the magnetic exchange coupling constant, the dinuclear structure is modelled with the spin Hamiltonian:

$$\hat{H} = -2J\hat{S}_1\hat{S}_2 = -J(\hat{S}_T^2 - \sum_{i=1}^{2}\hat{S}^2)$$

$$\chi = \frac{Ng^2\beta^2}{3kT} \times \frac{\begin{array}{l}8976e^{272J/kT} + 7440e^{240J/kT} + 6090e^{210J/kT} + 4914e^{182J/kT} + 3900e^{156J/kT} \\ + 3036e^{132J/kT} + 2310e^{110J/kT} + 1710e^{90J/kT} + 1224e^{72J/kT} + 840e^{56J/kT} \\ + 546e^{42J/kT} + 330e^{30J/kT} + 180e^{20J/kT} + 84e^{12J/kT} + 30e^{6J/kT} + 6e^{2J/kT}\end{array}}{\begin{array}{l}33e^{272J/kT} + 31e^{240J/kT} + 29e^{210J/kT} + 27e^{182J/kT} + 25e^{156J/kT} + 23e^{132J/kT} + 21e^{110J/kT} \\ + 19e^{90J/kT} + 17e^{72J/kT} + 15e^{56J/kT} + 13e^{42J/kT} + 11e^{30J/kT} + 9e^{20J/kT} \\ + 7e^{12J/kT} + 5e^{6J/kT} + 3e^{2J/kT} + 1\end{array}}$$

$$\chi_{Ho} = \frac{\chi}{1-(2zj'/Ng^2\beta^2)\chi}$$

In these expressions, J is magnetic exchange coupling constant, N, g, β, and k have their usual meanings, zJ' is the total exchange parameter. The best fitting of the susceptibility data in the temperature range 50–300 K gives J = -0.075 cm^{-1}, zJ' = -8.159×10^{-5} cm^{-1}, g = 1.235, R = $\Sigma[(\chi T)_{obsd}$ -

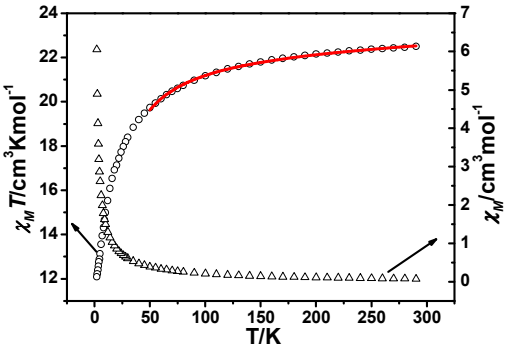

Fig. 5. Plots of $\chi_M T$ (○) and χ_M (△) vs. T for **2**. The red lines represent the fitting results.

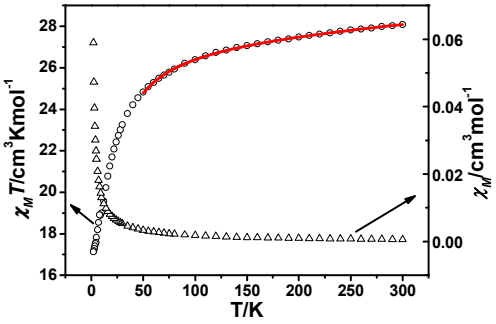

Fig. 6. Plots of $\chi_M T$ (○) and χ_M (△ vs. T for **3**. The red lines represent the fitting results.

$(\chi T)_{calcd}]^2/\Sigma[(\chi T)_{obsd}]^2 = 4.812\times10^{-7}$. The negative value of zJ' and θ indicate that an antiferromagnetic interactions between Ho^{3+} ions is operative.

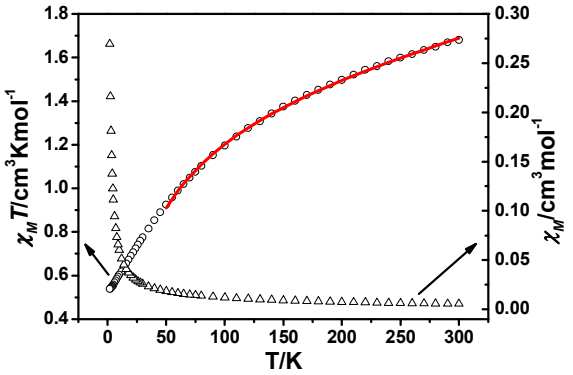

Fig. 7. Plots of $\chi_M T$ (○) and χ_M (△vs. T for **4**. The red lines represent the fitting results.

$[Nd(H_2ASA)(HASA)(H_2O)_4]$ (4). The temperature dependence of magnetic susceptibility for **4** is studied and shown in Fig. 7, and the $\chi_M T$ value at 300 K is 1.68 cm^3 K mol^{-1}, which is agreement with the expected value of 1.68 cm^3 K mol^{-1} for an uncoupled Nd^{3+} ion ($^4I_{9/2}$, S = 3/2, L = 6, g = 4/5, $\chi_M T$ = 1.68 cm^3 K mol^{-1}) in the ground state. Upon decreasing the temperature, the $\chi_M T$ value decrease continuously and reaches a minimum of 0.54 cm^3 K mol^{-1}, which may arise from the depopulation of Stark sublevels and/or antiferromagnetic interaction between Nd^{3+} ions.[17] A nonlinear fit via [χ_M = C/(T - θ) + χ_0] in the temperature range 50-300 K gives the Curie constant C = 1.475 cm^3 K mol^{-1}, the Weiss constant θ = -37.008 K, and the background susceptibility χ_0 = 0.00125 cm^3 mol^{-1}, R = $\Sigma[(\chi T)_{obsd} - (\chi T)_{calcd}]^2/\Sigma[(\chi T)_{obsd}]^2$=1.263×10^{-5}. The negative value of θ indicates the presence of weak antiferromagnetic interactions between Nd^{3+} ions.

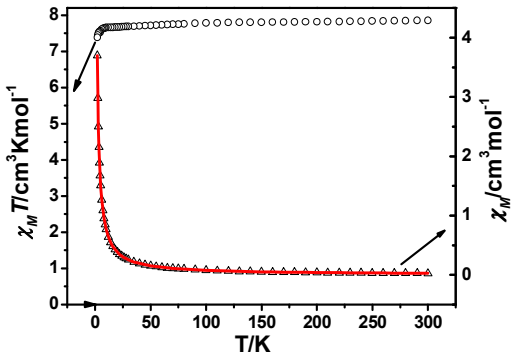

Fig. 8. Plots of $\chi_M T$ (○) and χ_M (△vs. T for **5**. The red lines represent the fitting results.

$[Gd(H_2ASA)(HASA)(H_2O)_4]$ (5). For **5**, as the temperature is lowered from 300 to 90 K, the $\chi_M T$ value is almost constant with a small scale of 7.86 to 7.78 cm^3 K mol^{-1} which is close to the theoretical value for an uncoupled Gd^{3+} ion ($^8S_{7/2}$, S=7/2, L = 0, g = 2, $\chi_M T$ = 7.88 cm^3 K mol^{-1}). Below 90 K, $\chi_M T$ shows a sharp decrease with decreasing temperature to reach a value 7.38 cm^3 K mol^{-1} at 2 K. The reciprocal susceptibilities data ($1/\chi_M$) conforms well to Curie-Weiss law (χ_M = C/(T - θ)) in the range of 2-300 K and give the negative Weiss constant θ = -0.52 K and Curie constant C = 7.85 cm^3 K mol^{-1} (Fig S7, ESI†). These data, in combination with the changing tendency of $\chi_M T$-T, lead to the conclusion that the magnetic coupling between the neighbouring Gd^{3+} ions bridged by H_3ASA ligand is antiferromagnetic. The theoretical χ_M is given by the following expression, which is based on the spin Hamiltonian $H = -J\Sigma SiSi+1$ with the quantum numbers $S_{Gd} = 7/2$: [18]

$$\chi_{chain} = \frac{Ng^2\beta^2}{3kT}\frac{1+u}{1-u}S(S+1)$$

where $u = \coth(J_c S(S+1)/kT) - kT/J_c S(S+1)$

In these expressions, J_c is magnetic exchange coupling constant, S, N, g, β, and k have their usual meanings. The best fitting of the susceptibility data in the temperature range 2–300 K gives J_c = -0.0041 cm^{-1}, g = 1.979, R = $\Sigma(\chi_{obsd} - \chi_{calcd})^2/\Sigma(\chi_{obsd})^2$= 2.303×10^{-6}. The magnitude of J_c is small but is of the same order as other Gd^{3+} complexes.[19] The reason for this may be that the 4f electrons lie closer to the metal center than the 5d and 6s electrons and are less influenced by the surrounding environment. The negative value of J_c further confirms the antiferromagnetic coupling between the Gd^{3+} ions.

$\{[Dy(ASA)(H_2O)_5]\cdot5H_2O\}$ (6). As illustrated in Fig. 9, the $\chi_M T$ value for **6** at 300 K is 14.18 cm^3 K mol^{-1}, which is consistent with the expected value of 14.18 cm^3 K mol^{-1} for an uncoupled Dy^{3+} ion ($^6H_{15/2}$, S = 5/2, L = 5, g = 4/3, χT = 14.18 cm^3 K mol^{-1}). When the temperature is lowered, the $\chi_M T$ value decrease very slowly to 13.87 cm^3 K mol^{-1} at ca. 35 K. Below 35 K, $\chi_M T$ decreases rapidly down to 11.00 cm^3 K mol^{-1} at 2 K. The decreasing values of $\chi_M T$ is most likely due to depopulation of the Stark sublevels and/or antiferromagnetic interaction

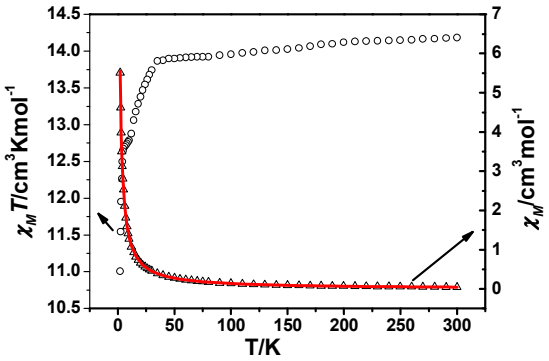

Fig. 9. Plots of $\chi_M T$ (○) and χ_M (△vs. T for **6**. The red lines represent the fitting results.

between Dy^{3+} ions. A nonlinear fit via $\chi_M = C/(T - \theta) + \chi_0$ in the temperature range 2–300 K Curie constant C= 13.849 cm^3 K mol^{-1}, Weiss constant θ = -0.498 K and the background susceptibility χ_0 = -0.0012cm^3 mol^{-1}, the agreement factor R = $\Sigma(\chi_{obsd}-\chi_{calcd})^2/\Sigma(\chi_{obsd})^2 = 1.27\times10^{-4}$. The negative value of θ indicates the presence of weak antiferromagnetic interactions between Dy^{3+} ions.

The photochromism of aqueous solution of 1-6

Fig. 10 gives the changes of UV-Visabsorption spectra of the alkaline aqueous solution of **1** with concentration of 2.0×10^{-5} mol·dm^{-3} under 365 nm UV light irradiation at room temperature. Upon irradiation of the alkaline aqueous solution of **1** with UV light (365 nm), the absorption peaks around 450 nm decrease in intensity and two absorption peaks around 260 and 350 nm increase in intensity and three regions with two isobestic points at 279 and 380 nm can be distinguished. When the UV light irradiation continuously increases for 15 minutes, the absorption intensity at 350 nm peak largely increase. When the time of UV light irradiation increases for 35 minutes, the original absorption peaks at 450 nm become unresolved. The phenomenon of maximum absorption peak transfer from 450 to 350 nm should be attributed to a photoisomeric reaction of anionic ligands (scheme 1).[8a] The alkaline aqueous solution of **2-6** show similar photochromic properties with **1** (Fig. S8, ESI†).

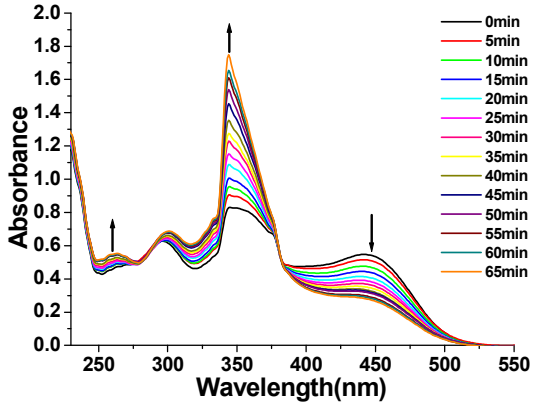

Fig. 10. UV-vis spectral changes of **1** in alkaline aqueous solutions with the concentration of 2.0×10^{-5} mol·dm^{-3} upon repeated irradiation at 365 nm at 5 min intervals at room temperature.

Conclusions

In summary, six novel lanthanide complexes based on H_3ASA ligand have been synthesized and reported. The H_3ASA has both π-system capable of forming π^-–π stacking interactions between tetrazolate anions and phenyl rings and the ability for formation of intra- and/or intermolecular hydrogen bonds. These supramolecular interactions are responsible for the stabilization of these 3D supramolecular structures. The magnetic and photochromic properties of these complexes were analysied and demonstrated. This study suggests that H_3ASA ligand can act as a good building block and may provide new insights into the design and assembly of varied supramolecular architectures.

Acknowledgements

This work was supported by the National Natural Science Foundation of China (No. 21271052), Science and Technology Program Foundation of Guangzhou (No. 2013J4100016) and Program Foundation of the second batch of innovation teams of Guangzhou Bureau of Education (13C04).

Notes and references

Analytical and Testing Center, Guangzhou Key Laboratory for Environmentally Functional Materials and Technology, Guangzhou University, Guangzhou 510006, P. R. China. E-mail: dw320@aliyun.com.

Electronic Supplementary Information (ESI) available: Cartesian coordinates of π^-–π stacking interaction in **1-6**, The results of π^-–π stacking interaction energies calculation of **1–6**, The atomic labelling diagram and crystal packing diagram of **3** and **5**, The diagram of hydrogen bonds in **1-6**, Plots of χ_M^{-1} vs. T for **5**, UV-vis spectra of **2–6** in alkaline aqueous solution, Difference-map plots of the azotetrazolyl rings for **1-5**, Crystallographic data in CIF format for **1–6** See DOI: 10.1039/b000000x/

1 (a) K. Binnemans, *Chem. Rev.,* 2009, **109**, 4283; (b) A. Dolbecq, E. Dumas, C. R. Mayer, P. Mialane, *Chem. Rev.,* 2010, **110**, 6009; (c)Cui, Y., Yue, Y., Qian, G., Chen, B. *Chem. Rev.* 2011, **112**, 1126; (d) J. Jiang, Y. Li, J. Liu, X. Huang, C. Yuan, X. W. D. Lou, *Adv. Mater.*, 2012, **24**, 5166; (e) C. Zou, Z.J. Zhang, X. Xu, Q.H. Gong, J. Li, C.-D. Wu, *J. Am. Chem. Soc.,* 2012, **134**, 87. (f) D. N. Woodruff, R. E. Winpenny, R. A. Layfield, *Chem. Rev.*, 2013, **113**, 5110; (g) P. Zhang, Y. N. Guo, J. Tang, *Coord. Chem. Rev.*, 2013, **257**, 1728. (h) C.-H. Zeng, F.-L. Zhao, Y.-Y. Yang, M.-Y. Xie, X.-M. Ding, D.-J. Hou, S. W. Ng, *Dalton Trans.*, 2013, **42**, 2052.

2 (a) R. Pardo, M. Zayat, D. Levy, *Chem. Soc. Rev.,* 2011, **40**, 672; (b) U. Schubert, *Chem. Soc. Rev.,* 2011, **40**, 575; (c) L. D. Carlos, R. A. S. Ferreira, V. Z. Bermudez, B. Julián-López, P. Escribano, *Chem. Soc. Rev.,* 2011, **40**, 536; (d) J. Ahn, S. Park, J. H. Lee, S. H. Jung, S.-J. Moon and J. H. Jung, *Chem. Commun.*, 2013, **49**, 2109; (e) P. A. Gale, N. Busschaert, C. J. E. Haynes, L. E. Karagiannidis and I. L. Kirby, *Chem. Soc. Rev.*, 2014, **43**, 205; (f) H.-J. Schneider, P. Agrawal and A. K. Yatsimirsky, *Chem. Soc. Rev.*, 2013, **42**, 6777.

3 (a) H. T. Chifotides and K. R. Dunbar, *Acc. Chem. Res.*, 2013, **46**, 894; (b) M. Stornaiuolo, G. E. De Kloe, P. Rucktooa, A. Fish, R. Elk, E. S. Edink, D. Bertrand, A. B. Smit, I. J. P. de Esch and T. K. Sixma, *Nat. Commun.*, 2013, **4**, 1875; (c) H. T. Chifotides, I. D. Giles and K. R. Dunbar, *J. Am. Chem. Soc.*, 2013, **135**, 3039; (d) J.-M. Lin, Y.-X. Qiu, W.-B. Chen, M. Yang, A.-J. Zhou, W. Dong and C.-E. Tian, *CrystEngComm*, 2012, **14**, 2779; (e) M. Yang, Z.-J. Ou Yang, W.-B. Chen, R.-F. Zhou, N. Li and W. Dong, *CrystEngComm*, 2013, **15**, 8529; (f) W.-B. Chen, Y.-X. Qiu, X.-M. Lin, M. Yang, H. Yan, F.-X. Gao, Z.-J. Ou Yang, W. Dong, *J. Coord. Chem.*, 2013, **67**, 1700.

4 (a) L. Adriaenssens and P. Ballester, *Chem. Soc. Rev.*, 2013, **42**, 3261; (b) X.-Z. Luo, X.-J. Jia, J.-H. Deng, J.-L. Zhong, H.-J. Liu, K.-J. Wang and D.-C. Zhong, *J. Am. Chem. Soc.*, 2013, **135**, 11684; (c) Y. Takezawa and M. Shionoya, *Acc. Chem. Res.*, 2012, **45**, 2066; (d) H. Schmidbaur, H. G. Raubenheimer and L. Dobrzański, *Chem. Soc. Rev.*, 2014, **43**, 345; (e) T. J. Wadas, E. H. Wong, G. R. Weisman and C. J. Anderson, *Chem. Rev.*, 2010, **110**, 2858.

5 (a) J. Heine and K. Müller-Buschbaum, *Chem. Soc. Rev.*, 2013, **42**, 9232; (b) D. J. Tranchemontagne, J. L. Mendoza-Cortés, M. O'Keeffe and O. M. Yaghi, *Chem. Soc. Rev.*, 2009, **38**, 1257; (c) H. W. Roesky and M. Andruh, *Coord. Chem. Rev.*, 2003, **236**, 91.

6 (a) L.-Z. Cai, M.-S.Wang, S.-H. Wang, P.-X. Li, G.-C. Guo, J.-S. Huang, *CrystEngComm*, 2013, **15**, 7670; (b) X. Feng, J. L. Chen, L. Y. Wang, S. Y. Xie, S. Yang, S. Z. Huo, S. W. Ng, *CrystEngComm*, 2014, **16**, 1334; (c) X. Feng, X. L. Ling, L. Liu, H. L. Song, L. Y. Wang, S. W. Ng, B. Y. Su, *Dalton Trans.*, 2013, **42**, 10292; (d) X. Li, H. L. Sun, X. S. Wu, X. Qiu, M. Du, *Inorg. Chem.*, 2010, **49**, 1865; (d) M. Chen, E. C. Sañudo, E. Jiménez, S. M. Fang, C. S. Liu, M. Du, *Inorg. Chem.*, 2014, **53**, 6708; (e) Z. H. Zhang, Y. Song, T. A. Okamura, Y. Hasegawa, W. Y. Sun, N. Ueyama, *Inorg. Chem.*, 2006, **45**, 2896; (f) Y. F. Liu, G. F. Hou, Y. H. Yu, P. F. Yan, J. Y. Li, G. M. Li, J. S. Gao, *Cryst. Growth Des.*, 2013, **13**, 3816.

7 (a) Y. Yang, P. Du, J. F. Ma, W. Q. Kan, B. Liu, J. Yang, *Cryst. Growth Des.*, 2011, **11**, 5540; (b) H. Wu, X.-W. Dong, H.-Y. Liu, J.-F. Ma, S.-L. Li, J. Yang, Y.-Y. Liu, Z.-M. Su, *Dalton Trans.*, 2008, 5331; (c) J. H. Thurston, A. Kumar, C. Hofmann, K. H. Whitmire, *Inorg. Chem.*, 2004, **43**, 8427; (d) F. Wiesbrock, H. Schmidbaur, *CrystEngComm*, 2003, **5**, 503; (e) F. Wiesbrock, H. Schmidbaur, *Inorg. Chem.*, 2003, **42**, 7283; (f) R. Murugavel, R. Korah, *Inorg. Chem.*, 2007, **46**, 11048; (g) M.-C. Yin, C.-C. Ai, L.-J. Yuan, C.-W. Wang, J.-T. Sun, *J. Mol. Struct.*, 2004, **691**, 33.

8 (a) W.-B. Chen, Z.-X. Li, X.-W. Yu, M. Yang, Y.-X. Qiu, W. Dong, and Y.-Q. Sun, *Dalton Tran.*, 2014, **43**, 9090; (b) J.-M. Lin, M. Yang, Y.-X. Qiu, W.-B. Chen, H. Yan, F.-X. Gao, Z.-J. OuYang, W. Dong and T.-C. Kuang, *ChemPlusChem,* 2013, **78**, 598.

9 (a) Y. Li, B. O. Patrick, D. Dolphin, *J. Org. Chem.*, 2009, **74**, 5237; (b) M. D. Segarra-Maset, P. W. N. M. Leeuwen, Z. Freixa, *Eur. J. Inorg. Chem.*, 2010, 2075; (c) P. Pratihar, T. K. Mondal, A. K. Patra, C. Sinha, *Inorg. Chem.*, 2009, **48**, 2760; (d) H. Nishihara, *Coord. Chem. Rev.*, 2005, **249**, 1468; (e) K. K. Sarker, D. Sardar, K. Suwa, J. Otsuki, C. Sinha, *Inorg. Chem.*, 2007, **46**, 8291; (f) J. Han, M. Maekawa, Y. Suenaga, H. Ebisu, A. Nabei, T. Kuroda-Sowa, M. Munakata, *Inorg. Chem.*, 2007, **46**, 3313.

10 (a) T. M. Klapotke and D. G. Piercey, *Inorg. Chem.*, 2011, **50**, 2732; (b) Y.-C. Li, C. Qi, S.-H. Li, H.-J. Zhang, C.-H. Sun, Y.-Z. Yu and S.-P. Pang, *J. Am. Chem. Soc.*, 2010, **132**, 12170; (c) J.-M. Lin, W.-B. Chen, X.-M. Lin, A.-H. Lin, C.-Y. Ma, W. Dong and C.-E. Tian. *Chem.Commun.,* 2011, **47**, 2402; (d) J.-M. Lin, Y.-X. Qiu, W.-B. Chen, M. Yang, A.-J. Zhou, W. Dong and C.-E. Tian, *CrystEngComm*, 2012, **14**, 2779; (e) W.-B. Chen, Y.-X. Qiu, X.-M. Lin, M. Yang, H. Yan, F.-X. Gao, Z.-J. Ou Yang, W. Dong, *J. Coord. Chem.*, 2013, **67**, 1700.

11 M. J. Frisch, G. W. Trucks, H. B. Schlegel, G. E. Scuseria, M. A. Robb, J. R. Cheeseman, G. Scalmani, V. Barone, B. Mennucci, G. A. Petersson, H. Nakatsuji, M. Caricato, X. Li, H. P. Hratchian, A. F. Izmaylov, J. Bloino, G. Zheng, J. L. Sonnenberg, M. Hada, M. Ehara, K. Toyota, R. Fukuda, J. Hasegawa, M. Ishida, T. Nakajima, Y. Honda, O. Kitao, H. Nakai, T. Vreven, J. A. Montgomery, Jr, J. E. Peralta, F. Ogliaro, M. Bearpark, J. J. Heyd, E. Brothers, K. N. Kudin, V. N. Staroverov, R. Kobayashi, J. Normand, K. Raghavachari, A. Rendell, J. C. Burant, S. S. Iyengar, J. Tomasi, M. Cossi, N. Rega, J. M. Millam, M. Klene, J. E. Knox, J. B. Cross, V. Bakken, C. Adamo, J. Jaramillo, R. Gomperts, R. E. Stratmann, O. Yazyev, A. J. Austin, R. Cammi, C. Pomelli, J. W. Ochterski, R. L. Martin, K. Morokuma, V. G. Zakrzewski, G. A. Voth, P. Salvador, J. J. Dannenberg, S. Dapprich, A. D. Daniels, O. Farkas, J. B. Foresman, J. V. Ortiz, J. Cioslowski and D. J. Fox, *GAUSSIAN 09* (Revision A. 02), Gaussian, Inc., Wallingford, CT, 2009.

12 (a) S. F. Boys and F. Bernardi, *Mol. Phys.*, 1970, **19**, 553; (b) N. Li, W.-B. Chen, Y.-F. Guan, Z.-J. OuYang and W. Dong, *Inorg. Chim. Acta*, 2014, **409**, 349.

13 I. L. Shegal, K. V. Stanovkina, N. G. Kovalenko and L. M. Shegal, *Khim. Geterotsikl. Soedin,* 1974, **10**, 369.

14 (a) R. N. Pribble and T. S. Zwier, *Science*, 1994, **265**, 75; (b) K. Liu, J. D. Cruzan and R. J. Saykally, *Science*, 1996, **271**, 929; (c) S. Maheshwary, N. Patel, N.Sathyamurthy, A. D. Kulkarni and S. R. Gadre, *J. Phys. Chem. A*, 2001, **105**, 10525; (d) Q. Y. Liu and L. Xu, *CrystEngComm*, 2005, **7**, 87; (e) S. K. Ghosh, P. K. Bharadwaj, *Angew. Chem., Int. Ed.*, 2004, **43**, 3577; (f) F. N. Dai, H. Y. He and D. F. Sun, *J. Am. Chem. Soc.*, 2008, **130**, 14064; (g) X. Wang, H. Lin, B. Mu, A. Tian and G. Liu, *Dalton Trans*, 2010, **39**, 6187; (h) Y.-C. Ou, Z.-J. Lin and M.-L. Tong, *CrystEngComm*, 2010,**12**, 4020.

15. A.-H. Yang, H.-L. Gao, J.-Z. Cui, B. Zhao, *CrystEngComm*, 2011, **13**, 1870.

16 (a) C. Janiak, *J. Chem. Soc., Dalton Trans.*, 2000, 3885; (b) A. Robertazzi, F. Krull, E. W. Knapp, and P. Gamez, *CrystEngComm*, 2011, **13**, 3293.

17. X. Zhang, N. Xu, S.-Y. Zhang, X.-Q. Zhao, P. Cheng, *RSC Adv.*, 2014, **4**, 40643.

18 M. E. Fisher, *Am. J. Phys*. 1964, **32**, 343.

19 (a) W. Shi, X.-Y. Chen, N. Xu, H.-B. Song, B. Zhao, P. Cheng, D.-Z. Liao, S.-P. Yan, *Eur. J. Inorg. Chem.,* 2006, 4931; (b) M. Hernandez-Molina, C. Ruiz-Perez, T. Lopez, F. Lloret, M. Julve, *Inorg. Chem.,* 2003, **42**, 5456.

Journal Name RSCPublishing

ARTICLE

Table 1 Crystal data and structure refinement for **1-6**

	1	**2**	**3**	**4**	**5**	**6**
formula	$C_{16}H_{33}ErN_{12}O_{18}$	$C_{32}H_{46}Er_2N_{24}O_{26}$	$C_{32}H_{46}Ho_2N_{24}O_{26}$	$C_{16}H_{17}N_{12}NdO_{10}$	$C_{16}H_{17}GdN_{12}O_{10}$	$C_8H_{23}DyN_6O_{13}$
Formula weight	848.80	1517.45	1512.79	681.66	694.67	573.82
Temperature/K	296(2)	296(2)	296(2)	296(2)	296(2)	296(2)
λ/Å	0.71073	0.71073	0.71073	0.71073	0.71073	0.71073
Crystal system	triclinic	triclinic	triclinic	monoclinic	monoclinic	monoclinic
Space group	Pī	Pī	Pī	Cc	Cc	$P2_1/c$
a/Å	12.9043(8)	9.7064(14)	9.6936(4)	16.2248(7)	16.3059(18)	10.8529(13)
b/Å	13.7369(8)	12.0080(17)	11.9920(4)	14.2682(6)	14.2088(16)	6.9013(9)
c/Å	18.1170(10)	12.7434(18)	12.8118(4)	10.0232(4)	10.0240(9)	27.181(3)
α/°	85.446(3)	110.523(6)	110.378(3)	90.00	90.00	90.00
β/°	77.264(3)	94.782(7)	94.930(4)	105.746(2)	105.473(6)	112.490(6)
γ/°	83.393(3)	105.108(7)	104.916(3)	90.00	90.00	90.00
Volume/$Å^3$	3106.9(3)	1317.6(3)	1323.48(8)	2233.28(16)	2238.3(4)	1881.0(4)
Z	4	1	1	4	4	4
$\rho_{calc}mg/mm^3$	1.815	1.912	1.898	2.027	2.061	2.026
m/mm^{-1}	2.797	3.272	3.076	2.410	3.048	4.050
F(000)	1700.0	750.0	748.0	1348.0	1364.0	1132.0
Reflections collected	47911	20387	20025	8855	8969	16013
Independent reflections	14304	6112	6153	5133	5107	4338
Flack parameters	—	—	—	0.050(2)	0.043(3)	—
Rint	0.0227	0.0245	0.0339	0.0273	0.0201	0.0418
Goodness-of-fit on F^2	1.036	1.037	1.045	1.039	1.069	1.005
Final R indexes [I>=2σ (I)]	$R_1 = 0.0249$, [a] $wR_2 = 0.0615$[b]	$R_1 = 0.0220$, $wR_2 = 0.0529$	$R_1 = 0.0337$, $wR_2 = 0.1015$	$R_1 = 0.0351$, $wR_2 = 0.0774$	$R_1 = 0.0262$, $wR_2 = 0.0620$	$R_1 = 0.0318$, $wR_2 = 0.0798$
Final R indexes [all data]	$R_1 = 0.0298$, $wR_2 = 0.0634$	$R_1 = 0.0244$, $wR_2 = 0.0539$	$R_1 = 0.0397$, $wR_2 = 0.1058$	$R_1 = 0.0405$, $wR_2 = 0.0805$	$R_1 = 0.0292$, $wR_2 = 0.0642$	$R_1 = 0.0429$, $wR_2 = 0.0944$

[a] $R = \sum||F_o|-|F_c||/\sum|F_o|$. [b] $wR_2 = [\sum w(F_o^2 - F_c^2)^2/\sum w(F_o^2)^2]^{1/2}$